Molecular dynamics simulations of passive transport in two-dimensional Rayleigh-Bénard convection

Stéphane Vannitsem
Institut Royal Météorologique de Belgique, 3, avenue circulaire, B-1180 Brussels, Belgium

Michel Mareschal
Chimie-Physique, Faculté des Sciences, Code Postal 231, Université Libre de Bruxelles, Brussels, Belgium
(Received 26 September 1994)

We use the molecular dynamics technique to study the enhancement of the self-diffusive transport of particles in a two-dimensional Rayleigh-Bénard convective fluid. The effective self-diffusion coefficient D^* can be computed from the simulations performed with 5 to 10 000 particles. The enhancement of diffusion with respect to molecular self-diffusion is shown to scale as $Pe^{1/2}$, where Pe is the Péclet number, which characterizes the ratio of the diffusive to the advective time. This behavior is in agreement with previous theoretical and experimental results. The simulation technique, however, permits us to explore domains of intermediate Péclet numbers around 100, where experiments are knowledgeably difficult to perform.

PACS number(s): 05.60.+w, 05.70.Ln, 44.25.+f, 47.27.Te

I. INTRODUCTION

The transport of matter in fluid systems is a process that finds important applications in various fields of science and engineering, including, for example, the dispersion of pollutants. The term passive that is sometimes added to it means that the velocity field of the fluid is not affected by the presence of the species that is transported: the tracer needs to be neutrally buoyant. The interplay between the small-scale random walk of the tracer particles, giving rise to the molecular diffusion processes, and the large-scale hydrodynamical flow field of the fluid is by no means trivial, as was shown for the first time by Taylor [1] in 1954.

Passive mass transport is of much interest in many complex situations, such as, for example, a fluid subject to turbulent motion or in flows in which spatiotemporal patterns have set in. These fluid states are themselves difficult to describe so that the modelization of the mass transport cannot be fully understood from the analysis of the basic starting equations: the Navier-Stokes equations for the fluid flow and the diffusion equation (in a fluid at rest) for the tracer. Phenomenological treatments, however, permit one to obtain most of the qualitative behavior of the scalar transport [2].

More recently, a lot of attention has been devoted to the understanding of passive mass transport when the fluid is undergoing a steady convective flow in a one-dimensional geometry. This is one of the simplest examples, where the interactions between diffusion and a steady flow structure can be examined in detail: indeed, an analytical form for the fluid flow field can be obtained from a perturbation expansion [3]. The nondimensional parameter characterizing the relative importance of the flow field mass transport and the molecular diffusion is given by the Péclet number Pe. This number is defined as the ratio $ul/D\pi$, with u a characteristic flow field velocity, l the typical length (in Rayleigh-Bénard convection experiments, l is the fluid layer height), and D the molecular diffusion coefficient. It is, as a matter of fact, the ratio of the diffusion-over-a-roll time over the inverse shear rate in the flow field.

Sagues and Horsthemke [4] have derived a diffusion equation for the tracer in the vicinity of the convective instability threshold, with an effective diffusion coefficient D^*. This result was later extended to the large Péclet number domain, so that the scaling of D^* with Pe has been derived in the whole Pe range [5], going from a Pe^2 behavior in the low Pe regime to a $Pe^{1/2}$ behavior at high Pe. In the limit of large Pe, Shraiman [6] and, independently, Rosenbluth *et al.* [7] have also found an enhancement of D proportional to $Pe^{1/2}$.

At large Pe, a crossover between two behaviors was predicted by Young, Pumir, and Pomeau [8], depending on the time scale investigated: for times smaller than the diffusion-over-a-roll time, no linear increase of the mean square displacement in time was found; rather, the number of convective cells invaded by the tracer was predicted to increase in time like $t^{1/3}$ for rigid and $t^{1/4}$ for stress-free boundary conditions [9,10]. For larger times, on the other hand, the diffusion law, with the number of invaded cells increasing like $t^{1/2}$, was recovered.

Experimental results have been reported by Solomon and Gollub [11]. They have found a diffusive behavior for impurities in a fluid layer with convective rolls in the direction perpendicular to the roll axis. Besides, over the range of Pe inspected—around a few hundred and around 10^6—they could confirm the square-root scaling behavior. Anomalous diffusion predictions were also tested and verified experimentally [12]. Numerous experiments have been reported concerning effective diffusion coefficients in turbulent media [13].

In this paper, we report a direct simulation by molecular dynamics (MD) of the passive diffusion in a Rayleigh-

 ©1995 The American Physical Society

Bénard cell. A few years ago, it was indeed found that the MD technique could be applied to the study of hydrodynamical instabilities [14]: fluid systems made of a few thousand particles, when submitted to the same constraints that would lead to the Rayleigh-Bénard instability, do indeed display the expected macroscopic behavior like the transition to the convective mode of heat transport. The solution obtained from the direct computation of the hydrodynamical variables from the MD simulation can quantitatively be compared to the solution obtained from the corresponding macroscopic analysis [15]. It is therefore tempting to use this molecular model to investigate the diffusive behavior in these models and to confront it with the theoretical predictions.

A fluid layer heated from below in the gravity field undergoes a transition to convective heat transport at a critical value of the Rayleigh number, Ra, which reads

$$\mathrm{Ra}=\frac{\alpha g \Delta T l^3}{\nu D_T} . \tag{1}$$

In Eq. (1) α is the thermal expansion coefficient, ν the kinematic viscosity, D_T the thermal diffusivity, g the gravity acceleration, and ΔT the temperature difference between the top and bottom of the layer. After the instability, the fluid develops a pattern, which, in an infinite horizontal geometry, is made of parallel rolls. This is in fact a two-dimensional structure in the plane perpendicular to the roll axis, which can be modeled by a two-dimensional microscopic simulation. Although the fluid layer height that can be achieved in a molecular simulation is fairly small, critical values of Ra (between 600 and 2000, depending on the boundary conditions) can be realized by an artificial increase of the forcing parameters g and ΔT. Any further increase of Ra can only be obtained by a corresponding increase of the number of particles used in the simulation.

During the last few years, several other problems arising in fluid mechanics have been examined through microscopic simulations [16,17]. Besides their fundamental interest regarding the limit of validity of the continuum theories, these simulations also furnish a complete description over different time scales of the fluid system of interest. In the present problem of diffusion in a Rayleigh-Bénard convective flow, they permit one to explore a range of values for the Péclet number that can hardly be reached in an experiment: between one and few tens. They also allow access to the full range of time scales, down from the molecular times up to the effective diffusion times.

This paper is organized as follows. In the following section, we present the method of molecular dynamics to model fluid flows. Then, we present the simulations performed for this study and discuss a little bit the stationary states obtained. The fourth section is devoted to the analysis of the behavior of the mean square displacements in time. Finally, along with our conclusions, we present a few remarks about possible extensions and limitations of this work.

II. THE MD TECHNIQUE

As is nowadays well known, most of the thermodynamic properties of a fluid can be reproduced from simple molecular dynamics models. In particular, away from the critical point, repulsive pair potential interactions between point particles allow one to simulate most of the fluid properties, both at and out of equilibrium.

Equilibrium properties can be obtained from simulations of systems made of a few hundred particles in periodic geometries. Periodicity is important, since it permits one to avoid the presence of perturbing boundary effects. In nonequilibrium stationary states (NESS), fluid systems respond to an external constraint by a flux of a transported quantity; this is often incompatible with periodic boundary conditions. Techniques have been developed in order to avoid boundary effects in NESS, too: the so-called Sllod (so called because of its close relationship to the Dolls tensor algorithm) and Evans-Gillan algorithms [18,19] are examples of methods that allow one to keep periodicity in a constrained fluid.

Here, however, we are interested in an inhomogeneous state; after the convective instability, a cellular flow field develops (rolls) in an external (gravity) field. This makes the presence of boundaries unavoidable, and therefore the simplest geometry chosen is the one displayed in Fig. 1.

For the reasons given above, in order to perform our simulations, we have chosen an ensemble of N point particles moving on a two-dimensional surface and interacting through a Weeks-Chandler-Anderson potential (see, for instance, Ref. [18]); that is,

$$V(r_{ij})=4\varepsilon\left[\left[\frac{\sigma}{r_{ij}}\right]^{12}-\left[\frac{\sigma}{r_{ij}}\right]^{6}\right]+\varepsilon \tag{2}$$

for $r_{ij}<2^{1/6}$ and zero otherwise. This corresponds to the Lennard-Jones potential cut at its minimum and shifted upward by its value at the corresponding distance. This model is well known to be sufficient to reproduce representative values of transport properties of fluids. Besides, the absence of attractive forces in the interactions leads, as in the case of hard spheres, to a solid-fluid phase diagram. No critical effects should perturb the evolution of the system.

The fluid particles are contained between two horizontal layers, the top ($y=L_y$) and bottom ($y=0$) boundaries, by an external potential that increases to infinity,

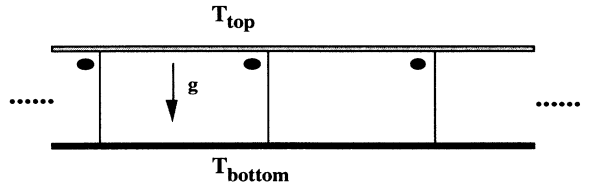

FIG. 1. Geometry of the simulation cell. The system is periodic in the horizontal (x-axis) direction, but constrained by two external fields in the vertical (y-axis) direction. Another external field accelerates particles downward, while two slices are thermalized at the top and the bottom of the fluid layer.

like the inverse twelfth power of the distance, so that the effect of this containing force is felt by the fluid particles over a distance of the order of σ. There is also another external force, $\mathbf{g}$, accelerating the fluid particles downward in order to mimic a gravitational force. The system is periodic in the horizontal (x-axis) direction so that the central cell is indefinitely repeated, as shown in Fig. 1. The fluid is also thermalized in two slices adjacent to the top and bottom boundaries. For reasons explained below, the thermalization mechanism is performed through the local Nosé-Hoover technique [20]: for the particles that belong to these slices, the equations of motion are modified by a coupling with a reservoir at temperature T_{top} or T_{bottom} and these two horizontal slices are divided into cells. At each time step the instantaneous number of particles N_α and the instantaneous cell velocity $\mathbf{u}_\alpha$ of cell α are computed from the values of the velocities of the particles belonging to that cell. For particles belonging to cell α, the equations of motion read

$$\frac{d\mathbf{p}_i}{dt}=\mathbf{F}_i+m\mathbf{g}-\zeta_{\text{NH}}\mathbf{p}_i\ , \tag{3a}$$

$$\frac{d\zeta_{\text{NH}}}{dt}=\frac{1}{\tau^2}\left[\frac{K-K_0}{K_0}\right]\ , \tag{3b}$$

$$\hat{K}=\sum_{i\in\alpha}\frac{(\mathbf{p}_i-m\mathbf{u}_\alpha)^2}{2m}\ , \tag{3c}$$

$$K_0=\frac{3(N_\alpha-1)}{2}k_B T_{\text{imposed}}\ . \tag{3d}$$

ζ_{NH} is the Nosé-Hoover friction constant that evolves according to Eq. (3b), in which the τ parameter is chosen once and for all. For the particles that belong to the bulk, that is, those that do not belong to any of these boundary layer cells, their equation of motion is simply Eq. (3a) with a vanishing Nosé-Hoover friction constant.

Other simulation parameters are fixed by the physical problem we want to solve. For instance, the boundary conditions (BC) that we want to simulate are stress-free. Indeed, critical values of the Rayleigh number are lower for these BC. The Rayleigh number that can be achieved in a MD simulation is proportional to the number of particles; this implies that the CPU time required is proportional to the square of the number of particles (at best), or, equivalently, to the square of Ra. Therefore, in order to keep the CPU time within reasonable limits, it is preferable to choose BC that favor a low-Ra critical value. This is why we do not constrain the tangential fluid velocity at the boundary. In the x direction, we adopt periodic BC; the minimum number of rolls required is therefore 2 so that the aspect ratio (L_x/L_y) has been set to exactly 2.

Since the fluid velocity can vary on the boundary, a local thermalization has to be set in: the boundary layers have been divided into cells with as few particles as possible. In every boundary cell, a different reservoir coupling is switched on. However, there has to be a sufficient number of particles within a boundary cell; indeed, every time a particle enters (or leaves) one of these cells, it produces a discontinuity in the local density and the local fluid velocity, and therefore also in the equations of motion. The effect of this discontinuity decreases with the number of particles contributing to N_α and to $\mathbf{u}_\alpha$. We found that around 40 particles per cell was enough to avoid any strong perturbation; the cell size extends therefore over 5σ in the vertical direction and 20σ in the horizontal direction.

As already mentioned, the fluid model we use is similar to a fluid made of hard spheres. The thermodynamics properties of a hard-sphere fluid are well understood [21]. For instance, the transport coefficients computed from the Enskog equation are surprisingly in good agreement with those computed from molecular simulations, even at large densities [22]. We have performed a few equilibrium simulations in order to validate this Enskog model. The results are listed in Table I. As in the remaining part of this paper, all results are given in system's units in which $\sigma=\varepsilon=1$ and the mass of the particles $m=48$. The self-diffusion coefficient has been computed from the slope of the linear increase of the mean square displacement of the particles, while viscosity and thermal conductivity have been obtained through their Green-Kubo expressions [22,23]. The fluid was thermalized by a Nosé-Hoover thermostat at $k_B T=1$ and the number density $n=0.7$, well inside the fluid region.

The choice of temperature (or mean vertical temperature in nonequilibrium) is rather arbitrary, as it is for a hard-sphere fluid where temperature simply rescales the time variable. The choice of (mean) density, on the contrary, is determined by the two following requirements: it should be in a domain where the transport coefficients are small and the fluid should be considered as incompressible (in the sense of the Oberbeck-Boussinesq approximation).

The first requirement follows from the form of the Rayleigh number. Replacing the coefficients of Eq. (1) by their values for the model used (the Carnahan-Stirling equation of state for α and Enskog values of the viscosity and thermal diffusitivity), and keeping in mind that $mgl\approx k_B\Delta T$, Ra can be put in the form of a function of the density and temperature times N (see Ref. [15] for more details). N and $k_B\Delta T$ fixed, Ra is maximum for densities between $n=0.2$ and 0.4. In order to simulate an incompressible fluid, on the other hand, the speed of sound should be made as large as possible so that the largest possible density (around 0.4) seems the most appropriate. This leads to an estimate of $\text{Pe}\approx 10$; other choices, com-

TABLE I. Computed and reference values of the transport coefficients in the model fluid. The reference value is computed from the Enskog equation (first-order Chapmann-Enskog expression in two dimensions, see Ref. [22]).

Coefficient	Number density n	Computed value	Enskog value
Viscosity η	0.7	9.33	10.63
Thermal conductivity λ	0.7	0.91	0.98
Molecular self-diffusion D	0.4	0.09	0.055

patible with the simulation conditions, of the density and of the number of particles permit one to simulate fluids in the range between Pe ≈ 1 and 100.

III. SIMULATIONS

We have performed five different simulations whose parameters are listed in Table II. The first four have been performed with 9800 particles at different Rayleigh and Péclet numbers, and a fifth one has been made with 5000 particles in order to check any size dependence of the results. For convenience, in Table II we also list the values of the diffusion time obtained from the values of the computed equilibrium transport coefficients; the advective time τ_c has been computed from an estimate of the typical fluid velocity.

The system was first started with a uniform density and temperature fixed to the average values we want to have: $n=0.4$ and $k_BT=1$. We integrate in time (the time step being 0.032) and follow the evolution of the velocity, density, and temperature fields. These are computed from both a time and space average in statistical cells: we have 40×20 of these cells, and values recorded inside these cells are averaged over a few thousand time steps. This time average is done in order to eliminate the thermal noise, which would otherwise be dominant. It is only after this averaging procedure that a smooth velocity pattern emerges: an interval of 50 000 time steps seems to be the minimum required to generate a regular field.

Figure 2 shows the velocity field that sets in after many transients. The stable pattern does not emerge immediately, and many intermediate states appear and disappear before stationarity is reached. This stage takes around 500 000 time steps, which is computationally costly; on a Cray YMP Computer this took around 50 000 s for the 9800-particle system. The other states were then started with an initial condition obtained from the final configuration of the first simulation. Transients were, however, also observed, but the time necessary to reach stability was somewhat reduced.

TABLE II. Parameters of the simulations performed. N is the number of particles for the simulation, k_BT_{top} and k_BT_{bottom} are the fixed temperatures of the top and bottom thermostats, l is the fluid total layer height, Ra is the estimated Rayleigh number, and τ_c and τ_{diff}, respectively, are the times required for a particle to move over a roll distance by advection and by diffusion. Pe is the estimated Péclet number.

N	k_BT_{bottom}	k_BT_{top}	l	Ra	τ_c	τ_{diff}	Pe
9 800	1.6	0.4	110.7	2 635	6500	136 161	21
9 800	1.65	0.35	110.7	3 902	4700	136 161	29
9 800	1.7	0.3	110.7	3 586	4300	136 161	32
9 800	1.8	0.2	110.7	4 684	3600	136 161	38
5 000	2.0	0.1	79.1	3 056	2800	69 520	25

In Fig. 2, it is also apparent that the fluid velocity is not constant along the streamlines. We found two reasons for this: First, the number density increases as the top boundary is approached. Because of mass conservation, this implies a reduced mean fluid velocity, which, in turn, induces the vertical asymmetry of the roll. Second, the two rolls do not have the same extent. The roll displayed in the center of the figure has a radius that is 20% smaller than the other roll, which is split between the two sides of the figure. This is an important fluctuation that lasts for the entire simulation time. This asymmetry leads to an upstream mass flow (at around $x=160$ in Fig. 2) taking place within a narrower pipe than the downstream flow. Therefore the upstream velocity is somewhat larger than the downstream one. The fluctuations are intrinsic in the MD system (as in a real fluid); however, the importance of the effect is fairly large and its reduction by further averaging, either in time or in space, cannot be easily imagined because of a huge computational cost.

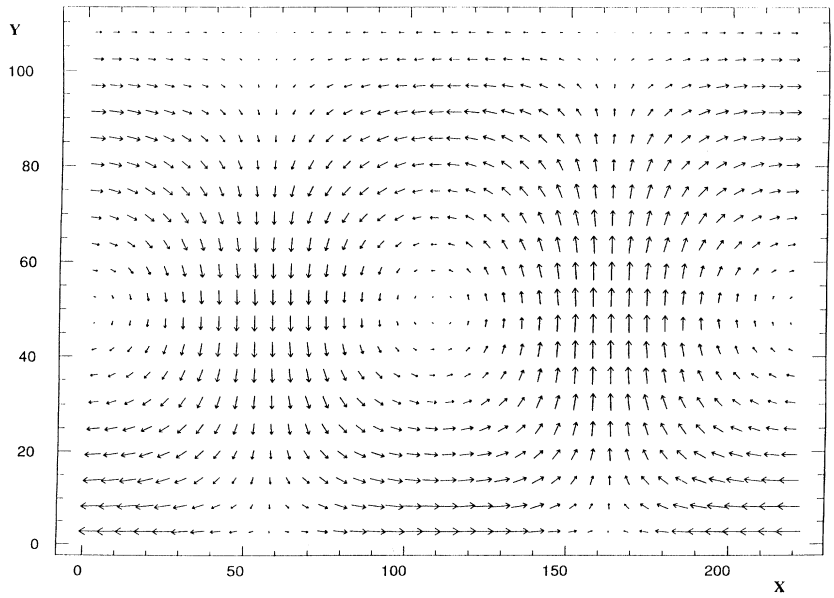

FIG. 2. Fluid velocity field after 10^6 time steps in the simulation performed with 9800 particles and $k_B\Delta T=1.4$. The pattern has been averaged over 700 000 time steps; intermediate time-averages over 100 000 time steps are very similar to the present figure.

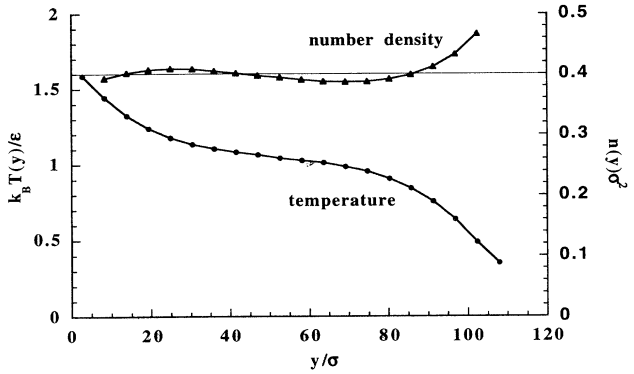

FIG. 3. Profiles versus height; the values are averaged over the horizontal direction.

Figure 3 displays the profiles of density and temperature averaged over the x direction as a function of the height. These profiles are very similar to those obtained in hard-sphere fluid models. The Navier-Stokes equations, completed by the equation of state, the transport coefficients, and the boundary conditions of our model, can be solved numerically on the computer by a finite difference method (more details can be found in Ref. [15]). The macroscopic results so obtained are not distinguishable from those of the MD computation. Even the density variation near the upper boundary matches quantitatively the macroscopic profile, once a local value for the thermodynamic parameters is fed into the Navier-Stokes equations. It is worth mentioning that the effect of compressibility is negligible and that the profiles look unchanged when the Boussinesq equations are used.

IV. DIFFUSION

The mean square displacements (MSD) in the x direction are shown in Fig. 4. The computations are performed with the real displacements along the x direction of every particle initially located in the unit cell of the simulation. The positions of the particles are recorded every 5000th step and the total durations of the runs were 750 000 steps. The correlations are kept over 500 000 time steps, and are displayed in Fig. 4.

One can distinguish three time scales corresponding to different behaviors:

(i) The first and shortest time scale is when molecular self-diffusion is dominant. This happens for very short times on the scale used for the plot ($t \approx 100$). The diffusion coefficients computed from the Einstein formula

$$\langle \Delta x^2(t) \rangle = 2Dt \tag{4}$$

compare well to their values computed from a periodic equilibrium system at the mean temperature and density.

(ii) Then the MSD start increasing much more than what is expected from molecular self-diffusion. For t of the order of 3000, there is a saturation and the rate of increase diminishes somewhat. This is the intermediate time scale when particles are accelerated by the flow field and then, later on, most of them come back near their original positions. This second stage is seen more clearly in Fig. 5, where the time derivatives of the MSD are plotted on the same time scale as the MSD of Fig. 4. From Fig. 5 it is clear that the time derivatives oscillate. These oscillations last up to $t \approx 5000$.

(iii) Finally, on the largest time scale, the MSD tend to become linear again, and the slope computed from the plot can be identified with twice an effective diffusion coefficient, D^*. Note however that, the larger the time, the more linear the increase of the MSD appears. Also, the higher the Rayleigh number, the sooner the linear regime starts.

In Fig. 6 we show a log-log plot of the MSD versus time during the last of these three periods. The linear fit

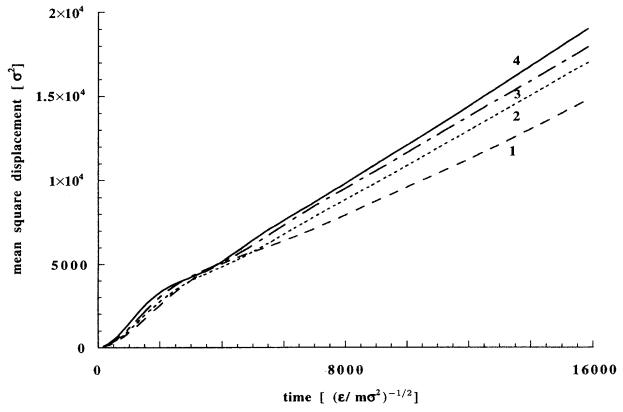

FIG. 4. Mean square displacements in the four simulations performed with 9800 particles: the time interval of the abscissa corresponds to 500 000 time steps, while the run length itself was 750 000 time steps. The curves are numbered by increasing Rayleigh number.

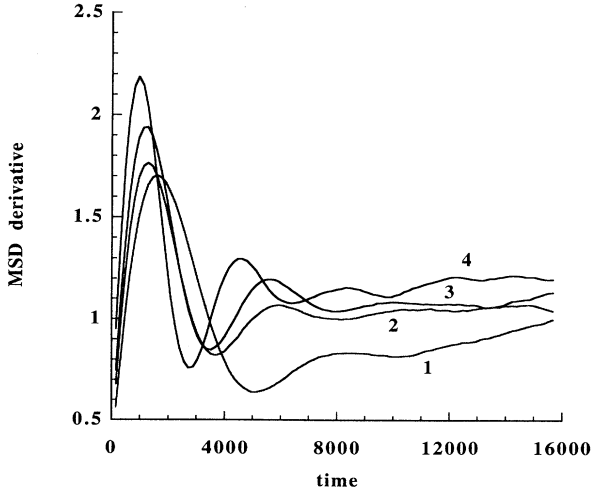

FIG. 5. Time derivative of the mean square displacements as a function of time. As in the previous figure, the numbers refer to the different simulations numbered by increasing Ra.

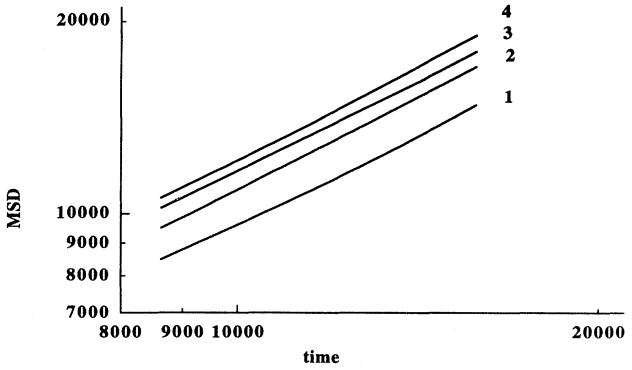

FIG. 6. Plot of the MSD against time in logarithmic scales. The curves are numbered in the same way as in the two previous figures.

of these graphs produces an angular coefficient around 1 within 3% if it is performed with the part of the graph between $t=12\,000$ and 16 000. Performing the fit from a time interval between 8000 and 16 000 increases the dispersion of the angular coefficients to around 10%. Quite clearly, the MSD reach the asymptotic regime of enhanced diffusion. The evaluation of D^* has been done by using Eq. (4) in the time interval between 12 000 and 16 000. It is to be stressed that the diffusive regime appears at relatively short times compared to τ_{diff}. This is probably the reason why the anomalous diffusion regime predicted in Refs. [8–10] is not found here: the range of Pe studied here is far from the large Pe limit where the anomalous regime is predicted.

The ratio D^*/D is plotted in Fig. 7 against the estimated Péclet number. The Péclet number can be written as the ratio of the diffusion time over the advective time $\tau_{\text{diff}}/\tau_c$. The diffusion times are listed in Table II for each simulation performed and have been obtained as the height to the square divided by the molecular diffusion coefficient. The advective time, on the other hand, has been computed from the oscillations occurring in the time derivatives of the MSD, as shown in Fig. 5; they are also listed in Table II. Indeed, the period of oscillation represents the average time needed for the fluid particles to perform one roll rotation on streamlines. Another estimate of Pe has been done by computing the fluid velocity on the separatrix between rolls. The result of this estimate is very similar to the one given in Table II and used in Fig. 7.

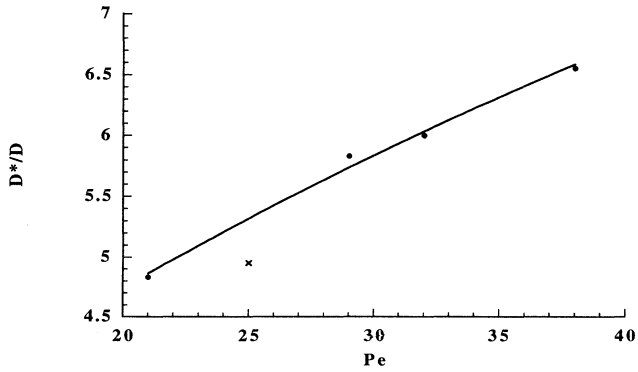

FIG. 7. Diffusion enhancement versus the Péclet number: the dots refer to the 9800 particle simulations and the cross corresponds to the $N=5000$ simulation. The curve is the a power-law fit on the $N=9800$ results.

We used the four points corresponding to the $N=9800$ simulations of Fig. 7 to make a power-law fit. The result of the estimate reads

$$D^*/D = 1.02\,\text{Pe}^{0.51}\,, \tag{5}$$

in relatively good agreement with the theoretical predictions. The square-root dependence is well reproduced in the MD computation. The value of the prefactor (as well as the estimated Pe), on the other hand, necessitates a much better precision for the D^* computation than the one which is obtained in such simulations. Indeed, we have not shown in Fig. 7 any error bars, since these are difficult to estimate. We believe that the only way to perform such an estimate would be to repeat similar independent computations and to observe the dispersions of the results, since the basic fluctuations are the very slow changes of the velocity patterns, which may take a fairly long time to average out.

The $N=5000$ results are qualitatively similar to those of the larger system. The behavior of the MSD, their time derivatives, and the diffusion enhancement are all equivalent to the behavior in the $N=9800$ particles system. However, the cross that appears in Fig. 7 is a little bit away from the curve fit. Although the mean values that are computed in this smaller system are also in quantitative agreement with the macroscopic description, the effect of the fluctuations can be expected to be more important. A smaller number of particles requires a larger time average to wipe out the effects of the thermal fluctuations. Even if the time to display the phenomenon is smaller in the $N=5000$ particles system, the integration time to reach the same precision of the diffusion coefficient might be larger.

V. CONCLUSIONS

We have succeeded in computing the diffusion enhancement of passive mass transport in a one-dimensional convective pattern directly from a microscopic modeling. The good comparison with the theoretical predictions can be viewed as either a kind of experimental test of the theory (since the modeling is at a fundamental level) or a confirmation of the ability of MD simulation to describe quantitatively hydrodynamic complex phenomena.

The CPU time required for the computations is, of course, quite large and may appear as the major limitation to the development of the application of the MD technique in this domain. Indeed, the improvement of both the precision and the variety of the physics observed depends strongly on N, the number of particles used in the simulation, and therefore on the computational cost.

For instance, the horizontal periodic boundary condi-

tions could be replaced by a much more extended system, so that a larger number of hydrodynamical vortices could be used to generate the data. Indeed, it has been seen, see Fig. 2, that the asymmetry of the rolls in the central cell was persisting on fairly large times. A more extended system could realize many more rolls and therefore leads to a much better hydrodynamical configurational average. Any increase in N will also lead to a better time resolution.

The Rayleigh number scales like N, while Pe scales like $N^{1/2}$. Therefore an increase of Pe by a factor of 10, all other things being equal, can be achieved by an increase by a factor of 100 of the number of particles. A larger size requires in turn an increase of the integration time (the latter being proportional to l^2/D; that is, N/D) to observe the physical phenomenon. Therefore the total CPU time required is multiplied by 10^4. A similar argument for the Rayleigh number leads to an increase of the CPU time by a factor 10^2. Under present conditions, it seems difficult to extend much the range of Pe or Ra by an N increase. The change in Pe and Ra can be easier to obtain from a change in the transport properties through the thermodynamic conditions or through the microscopic interparticle potential model.

A natural extension of this work could be a study by the MD technique of enhanced diffusion in various different complex flows, such as the successive transitions to turbulence in a thermal sheared fluids. A good example of these flows is the Kolmogorov model [24] where fully developed ($2d$) turbulence can be achieved with as few as 500 000 particles. At this moment the first instabilities can indeed be simulated by MD with around 10 000 particles. Further forseeable development of computational power makes it reasonable to reach turbulent states in the near future. Work in this direction is in progress and will be reported soon.

ACKNOWLEDGMENTS

We wish to thank Professor G. Nicolis for his constant encouragement. Financial support from the Belgian Government (Services Fédéraux des Affaires Scientifiques, Techniques et Culturelles, Contract No. IT/SC/27 and Global Change program) and the European Community are gratefully acknowledged.

[1] G. I. Taylor, Proc. R. Soc. London **219**, 186 (1953); **223**, 446 (1954); A **225**, 473 (1954). See also C. Van den Broeck, Physica A **168**, 677 (1990) for a recent review.
[2] H. K. Moffat, Rep. Prog. Phys. **46**, 621 (1983).
[3] S. Chandrasekhar, *Hydrodynamic and Hydromagnetic Stability* (Clarendon, Oxford, 1961).
[4] F. Sagues and W. Horsthemke, Phys. Rev. A **34**, 4136 (1987).
[5] P. McCarty and W. Horsthemke, Phys. Rev. A **37**, 2112 (1988).
[6] B. I. Shraiman, Phys. Rev. A **36**, 261 (1987).
[7] M. N. Rosenbluth, H. L. Berk, I. Doxas, and W. Horton, Phys. Fluids **30**, 2636 (1987).
[8] W. Young, A. Pumir, and Y. Pomeau, Phys. Fluids **A1**, 462 (1989).
[9] Y. Pomeau, A. Pumir, and W. R. Young, C. R. Acad. Sci. Ser. II **306**, 741 (1988).
[10] E. Guyon, J. P. Hulin, C. Baudet, and Y. Pomeau, Nucl. Phys. B **2**, 271 (1987).
[11] T. H. Solomon and J. P. Gollub, Phys. Fluids **31**, 1372 (1988).
[12] O. Cardoso and P. Tabeling, Europhys. Lett. **7**, 225 (1988).
[13] W. Y. Tam and H. L. Swinney, Phys. Rev. A **36**, 1374 (1987).
[14] M. Mareschal, M. Malek Mansour, A. Puhl, and E. Kestemont, Phys. Rev. Lett. **61**, 2550 (1988).
[15] A. Puhl, M. Malek Mansour, and M. Mareschal, Phys. Rev. A **40**, 1999 (1989).
[16] J. Koplik and J. R. Banavar, Annu. Rev. Fluid Mech. (to be published).
[17] For a recent review, see *Microscopic Simulation of Complex Hydrodynamic Phenomena* Vol. 292 of *NATO Advanced Science Institute, Series B: Physics Phenomena*, edited by M. Mareschal and B. L. Holian (Plenum, New York, 1992).
[18] D. J. Evans and G. P. Morriss, *Statistical Mechanics of Nonequilibrium Liquids* (Academic, London, 1990).
[19] W. G. Hoover, *Computational Statistical Mechanics* (Elsevier, Amsterdam, 1991).
[20] S. Nosé, Mol. Phys. **52**, 255 (1984); W. G. Hoover, Phys. Rev. A **31**, 1695 (1985).
[21] J. A. Barker and D. Henderson, Rev. Mod. Phys. **48**, 587 (1976); for transport properties of hard disks, see D. M. Gass, J. Chem. Phys. **54**, 1898 (1971).
[22] P. Résibois and M. DeLeener, *Classical Kinetic Theory of Fluids* (Academic, New York, 1977).
[23] P. M. Allen and D. J. Tildesley, *Computer Simulations of Liquids* (Clarendon, Oxford, 1987); B. J. Alder, D. M. Gass, and T. E. Wainwright, J. Chem. Phys **53**, 3813 (1970).
[24] G. I.Shivashinsky, Physica **17D**, 243 (1985); Z. S. She, Phys. Lett. A **124**, 161 (1987).